Kinetic Study of Hydrodechlorination of Chlorobiphenyl with Polymer-Stabilized Palladium Nanoparticles in Supercritical Carbon Dioxide

Weisheng Liao, Horng-Bin Pan, Hsin-Wang Liu, Hsing-Jung Chen, and Chien M. Wai*

Department of Chemistry, University of Idaho, Moscow, Idaho 83844

Received: January 28, 2009; Revised Manuscript Received: July 23, 2009

Hydrodechlorination of 4-chlorobiphenyl in supercritical fluid carbon dioxide (SF-CO_2) catalyzed by palladium nanoparticles stabilized in high-density polyethylene beads proceeds by consecutive reactions to the final product bicyclohexyl. Each step of the reaction sequence, that is, 4-chlorobiphenyl → biphenyl → cyclohexylbenzene → bicyclohexyl, follows pseudo-first-order kinetics. Arrhenius parameters of each reaction step were determined separately in SF-CO_2 by in situ absorption spectroscopy using a high-pressure fiber-optic cell. A simulation of product distributions using the first-order consecutive reaction equations was performed and compared with the experimental results obtained by GC/MS analysis of the 4-chlorobiphenyl reaction system. The differences are explained in terms of adsorption/desorption behavior of the intermediates on the catalytic metal surface with respect to the stereostructures of the molecules generated by a molecular mechanics method.

Introduction

Homogeneous and heterogeneous catalysis in supercritical fluids have drawn considerable attention since the early 1990s because of their potential advantages over conventional solvent systems including enhanced mass and heat transfer, control of selectivity, tunable solvation ability, extended catalyst lifetime, and minimization of liquid waste generation.[1−3] Carbon dioxide is the most widely used gas for supercritical fluid studies because of its mild critical constants (P_c = 72.8 atm and T_c = 31.1 °C), nontoxic nature, and low cost.[4−7] In a previous study, we demonstrated that toxic polychlorinated biphenyls (PCBs) could be converted to benign bicyclohexyl in SF-CO_2 via hydrogenation reactions catalyzed by palladium (Pd) nanoparticles stabilized in high-density polyethylene beads (Pd/HDPE).[8,9] The highly efficient catalytic hydrogenation reactions are attributed to several factors including relatively uniform distribution of nanometer-sized Pd particles in the polymer matrix, swelling of the polymer in SF-CO_2 allowing easy access of the reactants to the nanoparticle catalyst in the polymer matrix, and miscibility of hydrogen gas with SF-CO_2. In addition, the polymer-stabilized Pd nanoparticle catalyst can be reused many times without losing its activity. This type of reaction system satisfies not only sustainable chemistry but also economical requirements for advanced chemical processes development. Understanding basic knowledge of the catalytic hydrogenation reactions including kinetics and mechanisms of interactions between the catalyst and the reactants is essential for further development of effective catalysts for supercritical-fluid-based reactions. The catalytic conversion of PCBs to bicyclohexyl by hydrogen has been shown to proceed via the following first-order consecutive reactions[9]

$$\text{PCB} \rightarrow \text{biphenyl} \rightarrow \text{cyclohexylbenzene} \rightarrow \text{bicyclohexyl} \quad (1)$$

Kinetic parameters including rate constants at different temperatures and activation energies of the consecutive reactions catalyzed by the polymer stabilized Pd nanoparticles in SF-CO_2 are not known.

Kinetic studies of chemical reactions in SF-CO_2 are more difficult to perform than conventional systems because SF-CO_2 reactions are typically conducted under a relatively high pressure. Post reaction analysis via chromatography is a simple analytical technique used by a number of investigators for kinetic studies in supercritical fluids.[10−15] Using this technique, however, data collection may be tedious, and details of the chemical processes under investigation may not be totally revealed. In situ spectroscopic techniques are more suitable for kinetic studies in SF-CO_2. A high-pressure fiber-optic cell connected to a UV/vis spectrometer with a charge-coupled device (CCD) array was previously used by our group for solubility measurements and for monitoring nanoparticle formation in SF-CO_2.[16−18] In the present study, the fiber-optic device was used for acquiring kinetic data of the reactions involved in hydrogenation of a PCB compound (4-chlorobiphenyl or BZ#3) catalyzed by HDPE-stabilized Pd nanoparticles in SF-CO_2. The kinetic information of each individual step shown in eq 1 was obtained via in situ UV/vis spectra. On the basis of the kinetic information obtained from each individual reaction, a simulation of product distributions versus time for the overall catalytic hydrogenation of the PCB was performed according to the equations known for first-order consecutive reactions. The simulated results are compared with the experimental data, and the differences are explained in terms of surface adsorption/desorption of the intermediate products formed in the consecutive reaction steps.

Experimental Section

Palladium hexafluoroacetylacetonate [Pd(hfa)$_2$] (>97%), high density polyethylene (HDPE) beads (circular flat white beads with average diameter, height, and weight of about 3 mm, 1.5 mm, and 14 mg, respectively), biphenyl, cyclohexylbenzene, bicyclohexyl, and 4-bromobiphenyl (as a GC/MS internal standard) were purchased from Aldrich (Milwaukee, WI). Liquid carbon dioxide (>99.99%) and H_2 gas were supplied by Oxarc

* Corresponding author. E-mail: cwai@uidaho.edu.

10.1021/jp9008459 CCC: $40.75
Published on Web 08/17/2009

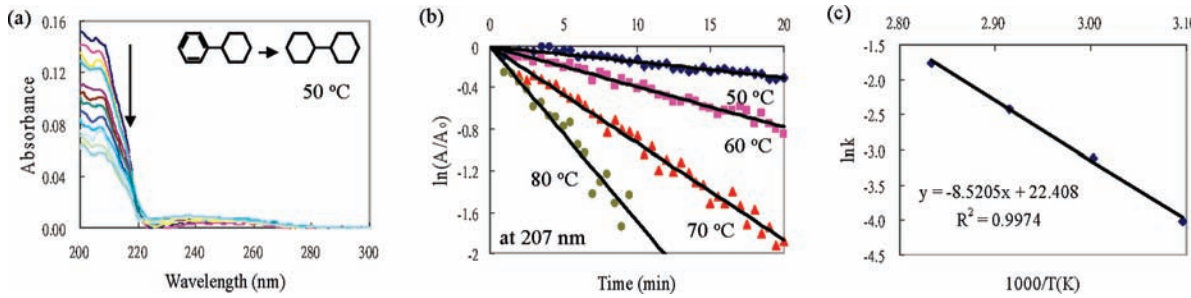

Figure 1. (a) Full UV/vis spectra, (b) $\ln(A/A_0)$ versus time plot at 207 nm, and (c) Arrhenius plot of Pd/HDPE-catalyzed hydrogenation of cyclohexylbenzene to bicyclohexyl in SF-CO_2.

(Spokane, WA). 4-Chlorobiphenyl (BZ#3) was purchased from Ultra Scientific (North Kingstown, RI). HPLC-grade hexane was purchased from Fisher Scientific (Fair Lawn, NJ). The pressure and temperature of the system were controlled by an ISCO syringe pump (model 260D, Lincoln, NB) with a series D pump controller and a Varian GC oven (model 3700, Palo Alto, CA). All high-pressure equipment was homemade or purchased from High Pressure Equipment Company (HiP, Erie, PA). A UV/vis spectrometer with CCD array (Model 440, Spectral Instruments, Tucson, AZ) connected to a high-pressure reactor via silicon optical fibers was used for in situ monitoring of chemical reactions in SF-CO_2. A GC/MS (model QP2010S, Shimadzu) with a DB-5 column was used to analyze samples for comparison with the UV/vis data. The synthesis and characterization of the Pd/HDPE catalyst are the same as those described in a previous publication.[8] Typically, the CO_2-soluble $Pd(hfa)_2$ precursor was introduced into HDPE beads via a supercritical impregnation process in a high-pressure cell at 100 atm and 90 °C for 3 h. After impregnation, the white HDPE beads became yellowish, indicating the presence of $Pd(hfa)_2$ in the beads. The $Pd(hfa)_2$ was reduced to zerovalent Pd by 10 atm hydrogen gas at 90 °C. After H_2 reduction, the color of the beads became black, indicating the formation of Pd nanoparticles throughout the HDPE beads. The beads were then cleaned by flushing with neat SF-CO_2 to remove impurities. On the basis of TEM (transmission electron microscope) pictures, the size distribution of Pd nanoparticles in HDPE beads was in the range of 2−10 nm with an average value of 5 nm, and Pd nanoparticles were mainly in the zero-valence state according to the XPS (X-ray photon spectroscopy) data.[8] The Pd concentration of the beads was about 430 ppm according to the result of neutron activation analysis. About 7.5×10^{-2} M of cyclohexylbenzene, biphenyl, and BZ#3 in hexane were separately prepared as stock solutions. The experimental procedure is described as follows. Basically, 10 μL of stock solution in a small beaker was placed in a 20 mL high-pressure reaction cell filled with about 5.4 g of Pd/HDPE at a designated temperature. After evaporation of hexane, the cell was pressurized with 100 atm of CO_2 to dissolve starting materials in advance. Subsequently, 200 atm of CO_2/H_2 mixture containing 10 atm of H_2 in a 20 mL H_2 storage cell was introduced to the reaction cell by pressure difference. UV/vis spectra were recorded via a fiberoptic device connected to the supercritical fluid reactor.[9] After each experiment, the system was cleaned with at least 30 mL of CO_2 with 1.0 mL/min of flow rate and checked by UV/vis spectra of the CO_2 phase to ensure there was no residue remaining in the system.

Results and Discussion

1. Catalytic Hydrogenation of Cyclohexylbenzene in SF-CO_2. The application of Pd/HDPE for chemical reactions in SF-CO_2 is based on the fact that polymers often swell in SF-CO_2.[8] The extent of swelling usually depends on CO_2 pressure, temperature, polymer molecular weight, identity of polymers, and so forth.[19] Under the SF-CO_2 environment, the mobility of polymer chains is greatly increased (plasticization), allowing relatively easy diffusion of reactants into polymer matrix to contact with embedded metal nanoparticles for chemical reactions. In addition, the dispersion of heterogeneous catalysts in a system plays an important role with respect to catalyst performance. In our experimental setup, the reactor is filled with the Pd/HDPE beads (diameter = 3 mm) within which metal nanoparticles are predispersed. This arrangement resembles homogenization of a heterogeneous catalysis leading to fast conversion of PCBs to bicyclohexyl in static and dynamic catalytic hydrodechlorination reactions in SF-CO_2.[8,9]

Figure 1a shows a typical UV/vis spectrum (top curve) of cyclohexylbenzene in SF-CO_2 at 50 °C. Bicyclohexyl has no absorption peak in the UV/vis spectrum. As the hydrogenation reaction proceeds, the absorption of cyclohexylbenzene in SF-CO_2 decreases with time, as shown in the spectra collected at 5 min intervals after the start of the reaction. Cyclohexylbenzene has two characteristic peaks, a strong absorption at 207 nm and a very weak absorption at 252 nm. The latter is about 30 times lower in absorbance relative to the former. The peak at 252 nm is not clearly visible under our experimental conditions because of its low molar absorptivity. The catalytic hydrogenation reaction was conducted at 200 atm total pressure with 10 atm H_2 and a fixed amount of the HDPE-stabilized Pd nanoparticle catalyst. The effect of hydrogen pressure on catalytic hydrogen of biphenyl using transition-metal catalysts in SF-CO_2 was reported by Hiyoshi et al. to follow first-order kinetics.[20] The amount of H_2 used in this study was in large excess (>300 times) relative to the reactants. Therefore, the partial pressure of H_2 was virtually a constant during the hydrogenation reactions.

Figure 1b shows $\ln(A/A_0)$ versus time plots for the experiments at four different temperatures, where A is the absorbance at time t and A_o is the absorbance at $t = 0$ measured at 207 nm. A linear relationship between $\ln(A/A_0)$ and time is observed in all four cases, suggesting that the reaction is pseudo-first-order in the temperature range 50−80 °C. The average rate constants (min^{-1}) based on triplicate experiments at each temperature are $(1.80 \pm 0.27) \times 10^{-2}$, $(4.45 \pm 0.36) \times 10^{-2}$, $(8.84 \pm 0.35) \times 10^{-2}$, and $(1.73 \pm 0.08) \times 10^{-1}$ at 50, 60, 70, and 80 °C, respectively.[9] The rate constant approximately doubles for every

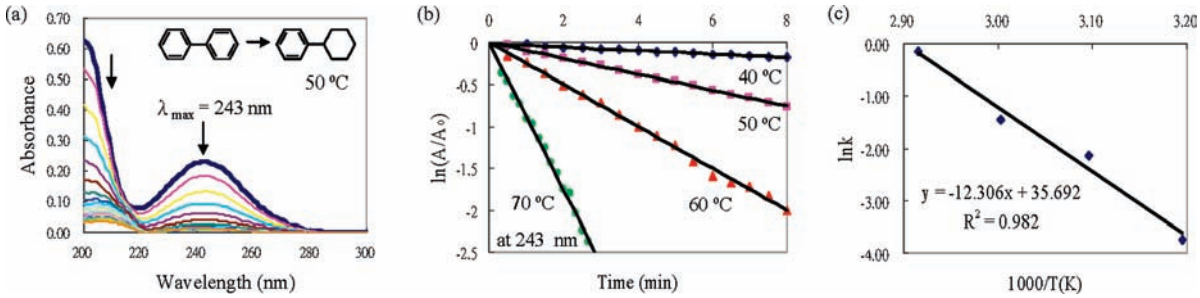

Figure 2. (a) Full UV/vis spectra of biphenyl, (b) $\ln(A/A_0)$ versus time plot at 243 nm, and (c) Arrhenius plot of Pd/HDPE-catalyzed hydrogenation of biphenyl in SF-CO_2.

10 °C elevation in temperature. The correlation coefficients (R^2) of all experiments are over 0.93. Yuan et al. has performed hydrogenation of some polyaromatic hydrocarbon over Pd/HDPE in SF-CO_2.[21] The authors pointed out that internal mass transfer resistance might be present in the Pd/HDPE, but the extent was not known. The influence of internal mass transfer resistance in our system was evaluated by the Thiele modulus and effectiveness factor.[22] The general equations for the Thiele modulus (Φ_o) and effectiveness factor (η) for a first-order reaction over spherical catalysts are shown in eqs 2 and 3, respectively

$$\Phi_o = L_p(k/D_e)^{1/2} \quad (2)$$

$$\eta = \tanh(\Phi_o)/\Phi_o \quad (3)$$

where L_p is the characteristic length parameter, k is the observed rate constant, and D_e is the effective diffusion coefficient.[22] The average rate constant obtained at 50 °C in the present study was used as an example. The effective diffusion coefficient of 4-chlorobiphneyl in Pd/HDPE in SF-CO_2 is not available in the literature. The effective diffusion coefficient of PCBs in sediment under SF-CO_2 condition was reported to be ca. 2.74×10^{-5} cm^2/s at 116 atm and 50 °C.[23] On the basis of this information, the Thiele modulus and effectiveness factor are calculated to be 0.331 and 0.965, respectively, indicating relatively small internal mass transfer resistance present in the heterogeneous catalytic system. The calculations are given in the Supporting Information.

Figure 1c is an Arrhenius plot of the rate constant versus the inverse of temperature ($1/T$), where T is the absolute temperature in Kelvin. The activation energy (E_a) calculated from the slope of the plot is 70.9 ± 2.6 (kJ/mol) with $R^2 = 0.997$ for the Pd/HDPE-catalyzed hydrogenation of cyclohexylbenzene to bicyclohexyl in SF-CO_2.

2. Catalytic Hydrogenation of Biphenyl in SF-CO_2. Figure 2a shows the UV/vis spectra of biphenyl (top curve) in SF-CO_2 at 50 °C and 200 atm taken at 5 min intervals after the start of the reaction. Biphenyl has an absorption peak at 243 nm, which is about 3 times lower in absorbance relative to that at 200 nm. During hydrogenation, biphenyl is converted to cyclohexylbenzene, which in turn is converted to bicyclohexyl. Both biphenyl and cyclohexylbenzene contribute to the absorptions at 200 and 243 nm. The peak at 243 nm can be used for acquiring the rate constant of the hydrogenation of biphenyl to cyclohexylbenzene because the contribution from cyclohexylbenzene to this peak is about 50 times lower than that of biphenyl and may be neglected. Figure 2b shows the $\ln(A/A_0)$ versus time plots at four different temperatures based on the absorbance measured at 243 nm. The $\ln(A/A_0)$ shows a linear relationship with time for all four temperatures, suggesting that the conversion of biphenyl to cyclohexylbenzene is also pseudo-first-order in nature. The average rate constants (min^{-1}) calculated from triplicate experiments at each temperature are $(2.37 \pm 0.06) \times 10^{-2}$, $(1.18 \pm 0.11) \times 10^{-1}$, $(2.36 \pm 0.15) \times 10^{-1}$, and $(8.53 \pm 0.44) \times 10^{-1}$ at 40, 50, 60, and 70 °C, respectively. The R^2 values of all plots are over 0.98. Figure 2c is the Arrhenius plot of the rate constants versus $1/T$. The E_a calculated from the slope is 102.3 ± 9.8 kJ/mol for Pd/HDPE-catalyzed hydrogenation of biphenyl to cyclohexylbenzene in SF-CO_2.

3. Catalytic Hydrodechlorination of 4-Chlorobiphenyl in SF-CO_2. Hydrodechlorination of 4-chlorobiphenyl leads to biphenyl and hydrogen chloride (HCl). Hunka et al. have studied the adsorption and desorption of HCl on Pd(111).[24] Three distinct HCl desorption states were evidenced, indicating that HCl generated during hydrodechlorination of 4-chlorobiphenyl in SF-CO_2 was not firmly adhered to the Pd surface but was continuously moving between the catalyst surface and the CO_2 phase. 4-Chlorobiphenyl has a characteristic absorption peak at 249 nm, whereas biphenyl absorbs at 243 nm, as described in the previous section. The molar absorptivity of the 249 nm peak from 4-chlorobiphenyl (23 000 Lcm^{-1}/mol) in SF-CO_2 is about 1.52 times greater than the 243 nm peak from biphenyl. During the catalytic hydrodechlorination process, the product biphenyl undergoes hydrogenation to cyclohexylbenzene and ends up as the saturated bicyclohexyl.

The UV/vis spectra obtained from the 4-chlorobiphenyl system during catalytic hydrogenation in SF-CO_2 are shown in Figure 3a. The absorption decreases with time, and the peak maximum is close to 249 nm with very little shift at 50 °C during the course of the hydrogenation process. This observation suggests that the absorption of biphenyl during the hydrodechlorination process is small compared with that of 4-chlorobiphenyl. A detectable shift in the absorption peak wavelength is observed for the hydrodechlorination reaction carried out at 60 °C, and the shift becomes significant for the reaction at 70 °C. Figure 3b shows the shift of the peak maximum (λ_{max}) versus time for the catalytic hydrodechlorination reaction at four different temperatures.

Although the contribution of biphenyl absorbance to its precursor is small between 40 and 60 °C, a correction is still needed to obtain reliable absorbance data for estimating the rate constants for the hydrodechlorination of 4-chlorobiphenyl. Herein we applied the method of least-squares, a commonly used technique for resolving two overlapping peaks, to separate the 4-chlorobiphenyl absorbance to that of biphenyl.[25] At first, five standard samples containing 4-chlorobiphenyl and biphenyl with different ratios were prepared to test the reliability of the method of least-squares for peak resolution. Different numbers of wavelengths were chosen, and a selection of five points gave

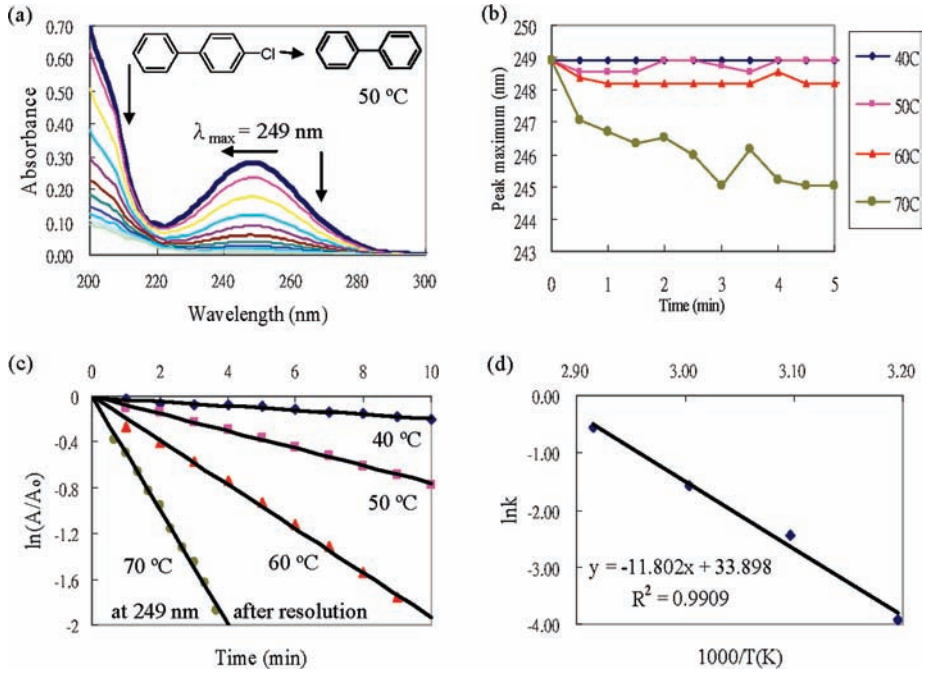

Figure 3. (a) Full UV/vis spectra of 4-chlorobiphenyl, (b) peak maximum shift versus time plot at 249 nm, (c) $\ln(A/A_0)$ versus time plot at 249 nm after resolution, and (d) Arrhenius plot of Pd/HDPE catalyzed HDC of BZ#3 in SF-CO_2.

TABLE 1: Kinetic Data for the Three Reaction Steps Involved in the HDC of BZ#3[a]

	BZ#3 to biphenyl	biphenyl to cyclohexylbeznene	cyclohexylbenzene to bicyclohexyl
k_{40}[b]	$(1.98 \pm 0.11) \times 10^{-2}$	$(2.37 \pm 0.06) \times 10^{-2}$	
k_{50}	$(8.01 \pm 0.57) \times 10^{-2}$	$(1.18 \pm 0.11) \times 10^{-1}$	$(1.80 \pm 0.27) \times 10^{-2}$
k_{60}	$(2.13 \pm 0.15) \times 10^{-1}$	$(2.36 \pm 0.15) \times 10^{-1}$	$(4.45 \pm 0.36) \times 10^{-2}$
k_{70}	$(6.06 \pm 0.83) \times 10^{-1}$	$(8.53 \pm 0.44) \times 10^{-1}$	$(8.84 \pm 0.35) \times 10^{-2}$
k_{80}			$(1.73 \pm 0.08) \times 10^{-1}$
R^2	>0.97	>0.98	>0.93
E_a[c]	100.5 ± 4.3	102.3 ± 9.8	70.9 ± 2.6

[a] Conditions: 200 atm of CO_2 including 10 atm of H_2 and 40−80 °C. [b] Unit = min^{-1}. [c] Unit = kJ/mol.

errors within 2%. Selection of less than five points resulted in larger errors, whereas selection of more than five points did not show a significant improvement. Therefore, five points, the peak maximum and ±7 and ±17 nm from the maximum, were chosen for the spectra resolution. The molar absorptivity values of BZ#3 and biphenyl at those points were obtained from the standards in SF-CO_2.

Figure 3c is an $\ln(A/A_0)$ versus time plot at four different temperatures after correcting the absorbance of 4-chlorobiphenyl at 249 nm. The plot indicates that the reaction is also pseudo-first-order. The observed average rate constants (min^{-1}) based on triplicate experiments are $(1.98 \pm 0.11) \times 10^{-2}$, $(8.01 \pm 0.57) \times 10^{-2}$, $(2.13 \pm 0.15) \times 10^{-1}$, and $(6.06 \pm 0.83) \times 10^{-1}$ at 40, 50, 60, and 70 °C, respectively. The R^2 values of these experiments are all over 0.97. Figure 3d is the Arrhenius plot, which shows an E_a value of 100.5 ± 4.3 (kJ/mol) for the Pd/HDPE-catalyzed HDC of BZ#3 to biphenyl in SF-CO_2. This is within the range of the E_a values reported for catalytic hydrodechlorination of PCBs using a sulfided Ni−Mo/Al_2O_3 catalyst.[26] The kinetic data for the three-step consecutive reactions are summarized in Table 1. The E_a values of biphenyl to cyclohexylbenzene and cyclohexylbenzene to bicyclohexyl step reactions are also within the E_a range reported for catalytic hydrogenation of biphenyl over Pd−Pt/Al_2O_3 in tetradecane free of external and internal mass transfer resistance.[27]

4. Simulation of Pd/HDPE-Catalyzed HDC of BZ#3 in SF-CO_2. For gas-phase consecutive first-order reactions involving four components (A → B → C → D), the variation in concentration of each component at a given time t can be expressed by the following equations[28]

$$[A] = [A]_o e^{-k_1 t} \quad (4)$$

$$[B] = [A]_o \{k_1/(k_2 - k_1)\}(e^{-k_1 t} - e^{-k_2 t}) \quad (5)$$

$$[C] = k_2[A]_o \{k_1/(k_2 - k_1)\}\{[1/(k_3 - k_1)](e^{-k_1 t} - e^{-k_3 t}) - [1/(k_3 - k_2)](e^{-k_2 t} - e^{-k_3 t})\} \quad (6)$$

$$[D] = [A]_o - [A] - [B] - [C] \quad (7)$$

Because Arrhenius parameters of each step of the Pd/HDPE-catalyzed HDC of BZ#3 in SF-CO_2 are known, the values of k_1, k_2, and k_3 at any temperature can be calculated for simulation. Figure 4a,b shows the simulated product distributions versus time at 50 and 70 °C based on the experimental Arrhenius parameters and the consecutive first-order reaction eqs 4−7. The simulation shows that the time required for converting 90% of BZ#3 to bicyclohexyl is about 30 min at 70 °C and 150 min at 50 °C. This is consistent with the experimental results obtained from GC/MS analysis of the samples taken from the catalytic hydrodechlorination of BZ#3 at different times. Another feature of the simulation is that the concentration of cyclohexylbenzene in the BZ#3 system is higher at 70 °C relative to that at 50 °C. This is expected because the E_a value for hydrogenation of cyclohexylbenzene is lower compared with the E_a value of its formation from biphenyl.

The results obtained from GC/MS analysis of product distributions in the SF-CO_2 phase for the catalytic hydrodechlorination of BZ#3 are shown in Figure 4c,d. Compared with the simulated plots (Figure 4a,b), some differences are obvious. A

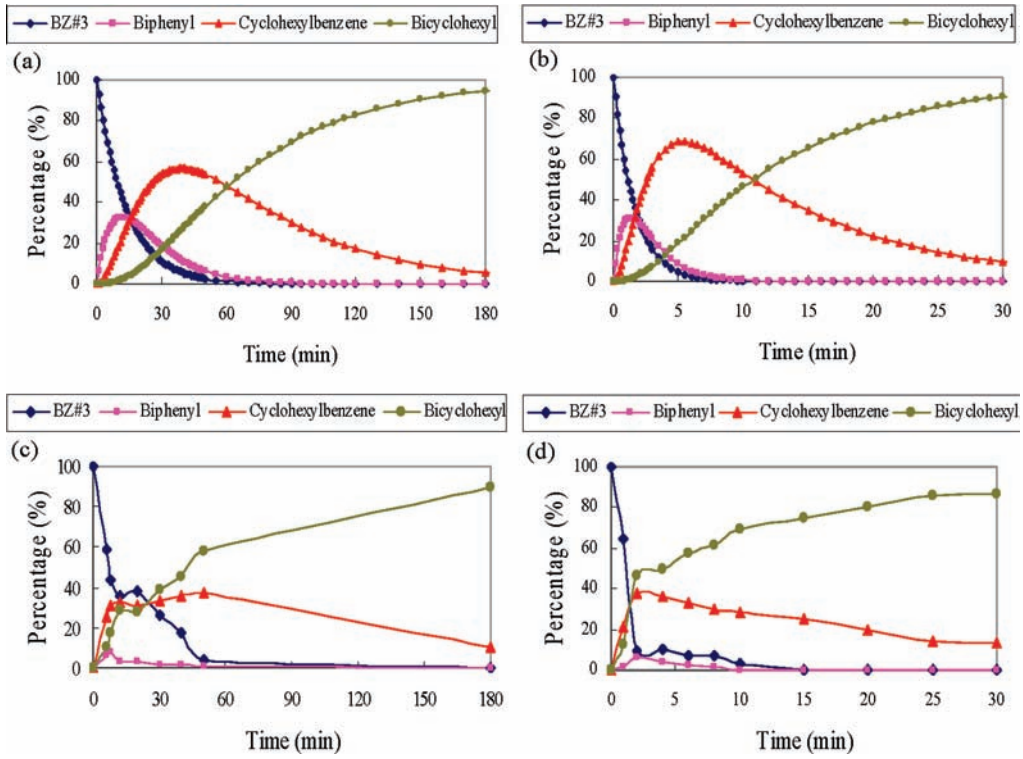

Figure 4. Product distribution with respect to time for Pd/HDPE-catalyzed HDC of BZ#3 in SF-CO_2 from simulation at (a) 50 and (b) 70 °C and from GC/MS analysis at (c) 50 and (d) 70 °C.

major difference is that the concentration of biphenyl in the SF-CO_2 phase observed experimentally in the BZ#3 system is much lower than the simulation prediction. This seems to suggest that biphenyl produced from hydrodechlorination of BZ#3 tends to stick to the catalyst surface and undergoes subsequent hydrogenation to cyclohexylbenzene. Consequently, the amount of biphenyl present in the SF-CO_2 phase is lower than that expected from the simulation. The distribution of cyclohexylbenzene in the SF-CO_2 phase is also lower than the simulation prediction but not as severe as the biphenyl distribution.

In a previous study of Pd/γ-Al_2O_3-catalyzed HDC of BZ#3 in hydrogen-saturated water, Schuth and Reinhard suggested that BZ#3 was directly converted to cyclohexylbenzene on the basis of their GC/MS analysis.[29] Bicyclohexyl was not detected until 7 h after the hydrodechlorination of BZ#3 according to that study. The rate constants for the hydrodechlorination of BZ#3 and the subsequent hydrogenation of biphenyl were reported to be $(4.78 \pm 0.05) \times 10^{-1}$ and $(5.55 \pm 0.02) \times 10^{-3}$ min^{-1}, respectively, at room temperature.[29] Further hydrogenation of cyclohexylbenzene was very slow (approximately 7 days for complete conversion), and no kinetic data were given by Schuth and Reinhard.[29] The rate constant for the hydrogenation of biphenyl in the hydrogen-saturated water system is about 50 times lower than the value observed in our SF-CO_2 system. The first step of the hydrodechlorination reaction is faster in the aqueous solution compared with our SF-CO_2 system probably because of the ease of removing HCl from the Pd surface in the aqueous environment.

The discrepancy in product distribution between the simulation and experimental observation may be attributed to the adsorption and desorption behavior of BZ#3 and the intermediate products formed in the hydrogenation processes. Morin et al. have calculated the adsorption energies of benzene, naphthalene, and anthracene on the platinum surface and shown that the adsorption energy tends to increase with increasing aromatic ring.[30] For example, the adsorption energies for benzene, naphthalene, and anthracene are −0.90, −1.37, and −1.79 eV/molecule, respectively. The authors divided the adsorption energy into three components, two distortion energies (positive) and one interaction energy (negative). When a molecule approaches a metal catalyst surface, the approaching molecule and the metal surface distort themselves for a better molecule-surface interaction. The energy required for this process is the distortion energy. The interaction energy between the distorted molecule and the distorted metal surface is the sum of the absolute value of adsorption energy (negative) and the distortion energies of the molecule and the surface. This concept may be used to explain the adsorption/desorption behavior of the molecules involved in the catalytic hydrodechlorination of BZ#3.

The stereostructures of 4-chlorobiphenyl, biphenyl, cyclohexylbenzene, and bicyclohexyl generated by the MM2 molecular mechanics method[31] with the function of energy minimization are shown in Scheme 1. Molecular orbital calculations can also give such information, but molecular mechanics calculations are generally easier, faster (require less computer time), and more accurate.[32] Therefore, the MM2 method is widely accepted by organic chemists for calculation of molecular conformational geometries.[33] Only the front views along the plane of the first benzene ring are shown in Scheme 1. The side views and top views are given in the Supporting Information (Scheme S1). As shown in Scheme 1, 4-chlorobiphenyl (far-left) has two planar benzene rings, and the angle between the two planes is about 46°. This stereostructure probably provides a suitable conformation for chemisorption on the catalyst surface with a relatively high adsorption energy and a low distortion energy. Consequently, k_a (adsorption rate constant) is presumably larger than k_b (desorption rate constant). As for biphenyl in Scheme 1 (middle-left), it also has two planar benzene rings, and the angles between two planes is 36°, which should provide an even more suitable conformation for chemi-

SCHEME 1: Proposed Mechanism of HDC of 4-Chlorobiphenyl on Pd Surface[a]

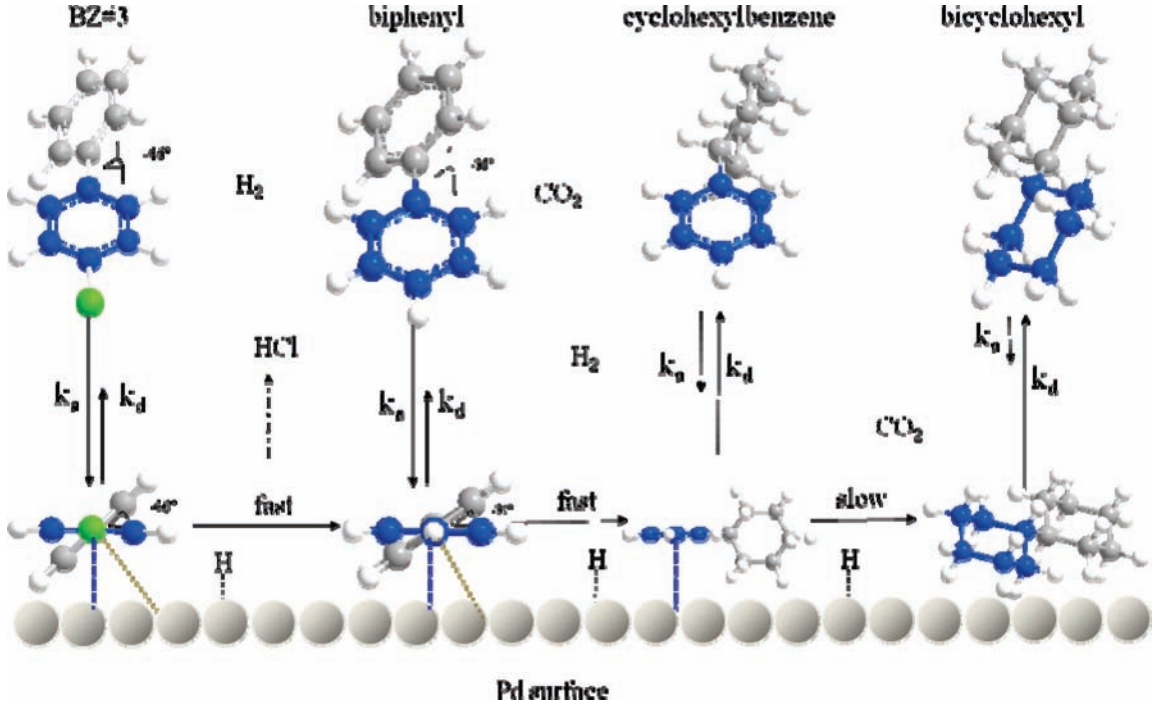

[a] k_a is the adsorption rate constant, whereas k_d is the desorption rate constant. The blue dash line (normal to the center of the benzene ring) implies that the benzene ring (blue) is adsorbed on the metal surface. The gray dotted line represents the benzene ring in the back (gray) that is tilted by 46° for 4-chlorobiphenyl and 36° for biphenyl to the metal surface. Structures are generated by the MM2 molecular mechanics method with energy minimization function. The molecules are viewed from the front at the same level as the blue benzene ring. The structure of each molecule on the catalyst surface is not the distorted form.

sorption on the catalyst surface because of the smaller plane angle. When 4-chlorobiphenyl is adsorbed on the Pd surface and reacted with H_2 to form biphenyl through HDC, most of the biphenyl molecules would probably proceed to the subsequent hydrogenation before it is desorbed from the metal surface. It is known that adsorbed hydrogen atoms are constantly hopping on catalyst surface before desorption takes place because of a lower activation energy of surface diffusion than that of adsorption.[34,35] The hydrogen source for the subsequent hydrogenation of biphenyl could be from either neighboring adsorbed hydrogen atoms or new hydrogen atoms from H_2 in the CO_2 phase. The net result is a low concentration of biphenyl in the SF-CO_2 phase compared with the simulation, which does not take adsorption/desorption into consideration. As for cyclohexylbenzene, it has one planar benzene ring and a chair-form cyclohexyl ring having a plane angle of about 90°. This stereostructure of cyclohexylbezene with hydrogen atoms sticking out above and below the benzene plane introduces significant steric hindrance for the chemisorption process and may obstruct the access of the migrated hydrogen atoms on the catalyst surface to the other benzene ring. When cyclohexylbenzene approaches the catalyst surface, it must distort itself to a more adequate conformation for successful chemisoprtion to take place, or it may simply bounce back. This high distortion barrier results in decreasing k_a and increasing k_d. In other words, the possibility of cyclohexylbezene adsorbed on the catalyst surface should be relatively low compared with that of 4-chlorobiphenyl and biphenyl. Consequently, most of the cyclohexylbenzene molecules that came from hydrogenation of biphenyl on the catalyst surface would desorb prior to further hydrogenation to bicyclohexyl, which has no strong interaction with the catalyst surface.

Conclusions

The results presented in this article demonstrate the feasibility of using a high-pressure fiberoptic device for studying the kinetics of catalytic HDC of a chlorobiphenyl compound in SF-CO_2. The kinetic parameters of the three consecutive reaction steps, 4-chlorobiphenyl to biphenyl, biphenyl to cyclohexylbenzene, and cyclohexylbenzene to bicyclohexyl, were measured separately. Each reaction step follows pseudo-first-order kinetics under our experimental conditions. The E_a values of the three step reactions are 100.5 ± 4.3 (kJ/mol) for 4-chlorobiphenyl to biphenyl, 102.3 ± 9.8 (kJ/mol) for biphenyl to cyclohexylbenzene, and 70.9 ± 2.6 (kJ/mol) for cyclohexylbenzene to bicyclohexyl. A simulation of product distributions with respect to time at different temperatures was performed using the gas-phase consecutive first-order reaction equations with the kinetic parameters obtained experimentally from each of the reaction steps. The simulated product distributions were compared with the experimental results obtained by GC/MS analysis of samples taken from the SF-CO_2 phase during the catalytic hydrodechlorination of the chlorobiphenyl. The calculated product distributions based on the consecutive first-order reaction equations show significant differences from the experimental data collected from the real reactions occurring in the SF-CO_2 phase. The discrepancy between the simulation and the experimental results may be explained in terms of the adsorption and desorption behavior of 4-chlorobiphenyl and its intermediate molecules formed on the catalyst surface during the hydrogenation process. The stereostructures of the molecules may be responsible for their adsorption/desorption behavior on the surface of the Pd metal nanoparticles.

Acknowledgment. This work was partially supported by AFOSR (FA9550-06-1-0526). H.-J.C. and H.-W.L. want to

thank National Chung-Hsing University and National Tsing-Hua University of Taiwan for financial support to study in the USA.

Supporting Information Available: The front-view pictures presented in Scheme 1 are from the MM2 simulation. Side views and top views of the molecules should help readers to have a clear understanding of the presented mechanism. This material is available free of charge via the Internet at http://pubs.acs.org.

References and Notes

(1) Savage, P. E.; Gopalan, S.; Mizan, T. I.; Martino, C. J.; Brock, E. E. *AIChE J.* **1995**, *41*, 1723.
(2) Baiker, A. *Chem. Rev.* **1999**, *99*, 453.
(3) Jessop, P. G.; Ikariya, T.; Noyori, R. *Chem. Rev.* **1999**, *99*, 475.
(4) Beckman, E. J. *J. Supercrit. Fluids* **2004**, *28*, 121.
(5) Leitner, W. *Acc. Chem. Res.* **2002**, *35*, 746.
(6) Subramaniam, B. *Appl. Catal., A* **2001**, *212*, 199.
(7) Burgener, M.; Ferri, D.; Grunwaldt, J.; Mallat, T.; Baiker, A. *J. Phys. Chem. B* **2005**, *109*, 16794.
(8) Liao, W.; Chen, Y. C.; Wang, J. S.; Yak, H. K.; Wai, C. M. *Ind. Eng. Chem. Res.* **2007**, *46*, 5089.
(9) Liao, W.; Takeshita, Y.; Wai, C. M. *Appl. Catal., B* **2008**, *88*, 173.
(10) Brock, E. E.; Oshima, Y.; Savage, P. E.; Barker, J. R. *J. Phys. Chem.* **1996**, *100*, 15834.
(11) Bertucco, A.; Canu, P.; Devetta, L.; Zwahlen, A. G. *Ind. Eng. Chem. Res.* **1997**, *36*, 2626.
(12) Anitescu, G.; Zhang, Z.; Tavlarides, L. L. *Ind. Eng. Chem. Res.* **1999**, *38*, 2231.
(13) Flores, R.; Lopez-Castillo, Z. K.; Kani, I.; Fackler, J. P., Jr.; Akgerman, A. *Ind. Eng. Chem. Res.* **2003**, *42*, 6720.
(14) Anitescu, G.; Tavlarides, L. L. *Ind. Eng. Chem. Res.* **2005**, *44*, 1226.
(15) O'brien, C. P.; Thies, M. C.; Bruce, D. A. *Environ. Sci. Technol.* **2005**, *39*, 6839.
(16) Carrott, M. J.; Wai, C. M. *Anal. Chem.* **1998**, *70*, 2421.
(17) Hunt, F.; Ohde, H.; Wai, C. M. *Rev. Sci. Instrum.* **1999**, *70*, 4661.
(18) Femandez, C. A.; Wai, C. M. *Small* **2006**, *2*, 1266.
(19) Royer, J. R.; DeSimone, J. M.; Khan, S. A. *Macromolecules* **1999**, *32*, 8965.
(20) Hiyoshi, N.; Rode, C. V.; Sato, O.; Shirai, M. *Appl. Catal., A* **2005**, *288*, 43.
(21) Yuan, T.; Marshall, W. D. *J. Environ. Monit.* **2007**, *9*, 1344.
(22) Davis, M. E.; Davis, R. J. *Fundamentals of Chemical Reaction Engineering*; McGraw-Hill: New York, 2003.
(23) Zhou, W.; Anitescu, G.; Tavlarides, L. L. *Ind. Eng. Chem. Res.* **2004**, *43*, 397.
(24) Hunka, D. E.; Herman, D. C.; Lopez, L. I.; Lormand, K. D.; Land, D. P. *J. Phys. Chem. B* **2001**, *105*, 4973.
(25) Harris D. C. *Quantitative Chemical Analysis*; W. H. Freeman & Company, New York, 2003.
(26) Murena, F.; Schioppa, E.; Gioia, F. *Environ. Sci. Technol.* **2000**, *34*, 4382.
(27) Castano, P.; Herk, D.; Kreutzer, M. T.; Moulijn, J. A.; Makkee, M. *Appl. Catal., B* **2009**, *88*, 213.
(28) Walas, S. M. *Chemical Reaction Engineering Handbook of Solved Problems*; Taylor & Francis: Amsterdam, 1995.
(29) Schuth, C.; Reinhard, M. *Appl. Catal., B* **1998**, *18*, 215.
(30) Morin, C.; Simon, D.; Sautet, P. *J. Phys. Chem. B* **2004**, *108*, 12084.
(31) (a) Allinger, N. L. *J. Am. Chem. Soc.* **1977**, *99*, 8127. (b) The MM2 molecular mechanics method is one of ChemBio 3D software's functions purchased from CambridgeSoft Corporation.
(32) (a) Osawa, E.; Musso, H. *Angew. Chem., Int. Ed.* **1983**, *22*, 1. (b) Boyd, D. B.; Lipkowitz, K. B. *J. Chem. Educ.* **1982**, *59*, 269. (c) Cox, P. J. *J. Chem. Educ.* **1982**, *59*, 275. (d) Levine, I. N. *Quantum Chemistry*, 5th ed.; Prentice Hall: Upper Saddle River, NJ, 2000. (e) Burkert, U.; Allinger, N. L. *Molecular Mechanics*; American Chemical Society: Washington, D.C., 1982.
(33) (a) Lipkowitz, K. B.; Peterson, M. A. *Chem. Rev.* **1993**, *93*, 2463. (b) Smith, M.; March, J. *March's Advanced Organic Chemistry: Reactions, Mechanisms, and Structure*, 5th ed.; Wiley: New York, 2001. (c) Carroll, F. A. *Perspectives on Structure and Mechanism in Organic Chemistry*; Brooks/Cole Pub. Co.: Pacific Grove, CA, 1998. (d) Eliel, E. L.; Wilen, S. H.; Mander, L. N. *Stereochemistry of Organic Compounds*; Wiley & Sons: New York, 1994.
(34) Ertl, G. *Angew. Chem., Int. Ed.* **2008**, *47*, 3524.
(35) Mitsui, T.; Rose, M. K.; Fomin, E.; Ogletree, D. F.; Salmeron, M. *Nature* **2003**, *422*, 705.

JP9008459